Phys. Status Solidi A **208**, No. 8, 1902–1907 (2011) / **DOI** 10.1002/pssa.201127010

physica status solidi a
www.pss-a.com
applications and materials science

Influence of etching process parameters on the antireflection property of Si SWSs by thermally dewetted Ag and Ag/SiO_2 nanopatterns

Jung Woo Leem[1], Jae Su Yu*[,1], Young Min Song[2], and Yong Tak Lee[2]

[1] Department of Electronics and Radio Engineering, Kyung Hee University, 446-701 Yongin, Republic of Korea
[2] Department of Information and Communications, Gwangju Institute of Science and Technology, 500-712 Gwangju, Republic of Korea

Received 10 January 2011, revised 24 March 2011, accepted 13 April 2011
Published online 4 May 2011

Keywords Ag nanoparticles, plasma etching, subwavelength structures, thermal dewetting, antireflective property

* Corresponding author: e-mail jsyu@khu.ac.kr, Phone: +82-31-201-3820, Fax: +82-31-206-2820

The etching parameter dependent antireflection characteristics of disordered Si subwavelength structures (SWSs) by inductively coupled plasma (ICP) etching in a mixture gas of $SiCl_4$/Ar using thermally dewetted Ag and Ag/SiO_2 nanopatterns are investigated. The average size and period of Si SWSs are closely correlated with thermal dewetting conditions. For desirable Ag nanoparticle patterns, the profile of Si SWSs is optimized by changing the ICP etching process parameters to obtain the lowest reflectance spectrum. The most tapered SWS with the highest height leads to a relatively low reflectance. The Ag nanopatterns result in more tapered and rough surface SWSs compared to the Ag/SiO_2 nanopatterns, indicating a slightly reduced reflectance. The Si SWS etched using Ag nanopatterns by $SiCl_4$/Ar of 5 sccm/10 sccm at 50 W RF power, 200 W ICP power, and 10 mTorr process pressure exhibits a very low total reflectance of $<\sim$2.4% in the wavelength range of 400–1000 nm, maintaining a specular reflectance of $<$16% at 350–1100 nm up to the incident angle of $\theta_i = 50^\circ$.

1 Introduction Antireflection coatings (ARCs) have been widely used to enhance the efficiency of optical components and optoelectronic devices including imaging cameras, sensor arrays, light emitting diodes, and solar cells [1–4]. Although single- or multilayer thin-films, such as SiO_x, TiO_x, or Si_xN_y, were employed to suppress the surface reflection loss, the conventional ARC techniques have given rise to several problems such as thermal expansion mismatch, stability, and material diffusion [5, 6]. Periodic subwavelength grating or disordered subwavelength structure (SWS) as an alternative has attracted much interest in recent years for various device applications [7–10]. The surface relief structure with a period smaller than the incident light wavelength can reduce the Fresnel reflection loss at the interface of two media by introducing a gradual change of refractive index [11]. However, the periodic grating structure needs complex and expensive nanolithography processes (i.e., e-beam lithography, nanoimprint lithography) for nanopatterns as an etch mask [12–14].

On the contrary, a simple, low-cost, and large-scale process for metallic nanoparticle patterns which are formed by the thermally activated dewetting of metastable thin metal films on a substrate can used to fabricate disordered SWSs [15–18]. The optical reflectance property of the SWS is directly related to the change in effective refractive index by the void volume fraction of the structure [19]. The shape and geometry of SWSs can be roughly controlled by varying the thermal dewetting and etching conditions. To achieve the antireflection property over a broadband spectrum, the etched profile of SWS should be properly optimized. In this paper, we investigated comparatively the structural and optical properties of disordered Si SWSs fabricated by optimizing the process conditions using thermally dewetted Ag and Ag/SiO_2 nanopatterns as the etch mask through the inductively coupled plasma (ICP) dry etching in $SiCl_4$/Ar mixture gas. The effect of light incident angle on the reflectance of the optimized Si SWS was also studied.

2 Experimental As the etch nanomasks for Si SWSs, the self-assembled Ag nanoparticles were fabricated on (100) Si and SiO_2/(100) Si substrates with a size of $2 \times 2\,cm^2$ by the thermal dewetting process of thin Ag films. The SiO_2 buffer layer of 50 nm was deposited on a Si substrate by a plasma enhanced chemical vapor deposition (PECVD, Plasmalab 80 Plus, Oxford) in SiH_4 (100 sccm)/N_2 (800 sccm) plasma at 20 W RF power and 1000 mTorr process pressure. The deposition temperature and time were 300 °C and 50 s, respectively. After wafer cleaning, the thin Ag films in the thickness range of 5–15 nm were evaporated with 99.99% purity Ag pellets by a thermal evaporator (KVE-T2000, Korea Vac. Tech. Ltd.) at a background pressure of $<2 \times 10^{-6}$ Torr. The evaporation rate was set to 0.1 nm/s as monitored by a quartz crystal oscillator. To form desirable Ag nanopatterns, the samples were heated at temperatures of 400–800 °C by a rapid thermal annealing (RTA, KVR-2000, Korea Vac. Tech. Ltd.) process under a nitrogen carrier flow rate of 10 sccm for 120 s. For the samples with a SiO_2 buffer layer, the SiO_2 layer was etched by a reactive ion etch (RIE, Plasmalab 80 plus, Oxford) system at 100 W RF power and 30 mTorr process pressure in 50 sccm CF_4 plasma for 60 s. A scanning electron microscope (SEM) image of this sample is shown in the inset of (vi) of Fig. 1. This process enables direct transfer of the thermally dewetted Ag nanopatterns on the underlying SiO_2 layer. By using the Ag and Ag/SiO_2 nanopatterns, the Si SWSs were fabricated by an ICP (Plasmalab System 100, Oxford) etching in $SiCl_4$/Ar plasma. The gas flow rates of $SiCl_4$/Ar were fixed to an optimum value of 5 sccm/10 sccm. For desirable etched profiles of Si SWSs, the etching process parameters, such as the RF power, ICP power, and process pressure, were changed. The RF power was varied from 25 to 100 W and the ICP power was changed from 0 to 200 W. The process pressure was also changed between 5 and 20 mTorr.

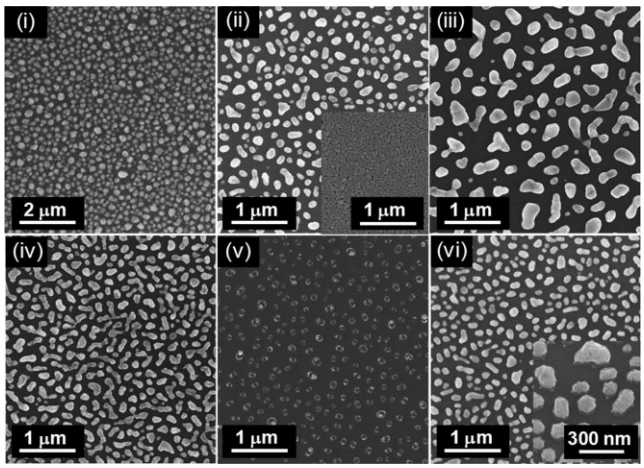

Figure 1 SEM images of the thermally dewetted Ag nanopatterns after RTA at 600 °C for Ag films of (i) 5 nm, (ii) 10 nm, and (iii) 15 nm and after RTA at (iv) 400 °C and (v) 800 °C for Ag films of 10 nm. The inset of (ii) shows the SEM image of 10 nm Ag film evaporated on a Si substrate before RTA. For comparison, the SEM image of the thermally dewetted Ag/SiO_2 nanopattern after RTA at 600 °C for 10 nm Ag film is also shown in (vi).

The etching time was fixed to 10 min. After the etching process, all samples were first dipped into heated nitric acid (HNO_3) solution and then into a buffered oxide etch solution for the Ag/SiO_2 masked samples to remove remaining Ag and SiO_2 residues, respectively. The process parameters of the fabricated samples, including the Ag film thickness, mask type, RTA temperature, RF power, ICP power, and process pressure, are summarized in Table 1. By a SEM (Carl Zeiss, LEO SUPRA 55) operating at 10 kV, the etched profile, etched depth, and surface morphology of the fabricated Si SWSs were observed.

Table 1 Process parameters of the fabricated Si SWSs.

samples	Ag film thickness (nm)	mask type	RTA temperature (°C)	RF power (W)	ICP power (W)	process pressure (mTorr)
S1	5	Ag	600	50	100	10
S2	10	Ag	600	50	100	10
S3	15	Ag	600	50	100	10
S4	10	Ag	400	50	100	10
S5	10	Ag	800	50	100	10
S6	10	Ag/SiO_2	600	50	100	10
S7	10	Ag	600	25	0	10
S8	10	Ag	600	50	0	10
S9	10	Ag	600	100	0	10
S10	10	Ag/SiO_2	600	25	0	10
S11	10	Ag/SiO_2	600	50	0	10
S12	10	Ag/SiO_2	600	100	0	10
S13	10	Ag	600	50	200	10
S14	10	Ag/SiO_2	600	50	200	10
S15	10	Ag	600	50	100	5
S16	10	Ag	600	50	100	20
S17	10	Ag/SiO_2	600	50	100	20

3 Results and discussion Figure 1 shows the SEM images of the thermally dewetted Ag nanopatterns after RTA at 600 °C for Ag films of (i) 5 nm, (ii) 10 nm, and (iii) 15 nm and after RTA at (iv) 400 °C, and (v) 800 °C for Ag films of 10 nm. The inset of (ii) in Fig. 1 shows the SEM image of 10 nm Ag film evaporated on a Si substrate before RTA. For comparison, the SEM image of the thermally dewetted Ag/SiO_2 nanopattern after RTA at 600 °C for 10 nm Ag film is also shown in (vi) of Fig. 1. The thin Ag films were agglomerated into nanoparticles by the thermal dewetting process via the RTA because of its enhanced surface energy at elevated temperatures [20]. The geometry of Ag and Ag/SiO_2 nanopatterns can be roughly controlled by both Ag film thickness and RTA temperature. The average correlation distance between Ag nanoparticles was increased and their sizes got bigger with the increase of Ag film thickness from 5 to 15 nm. By a commercial image processor (ImageJ 1.42q, NIH), the average diameter and correlation distance of Ag nanoparticles were estimated as 51.2 and 43.4 nm with an area fraction of 37.8% for 5 nm Ag film and 377.2 and 394.3 nm with 25.4% for 15 nm Ag film, respectively, after RTA at 600 °C. After RTA at 400 °C for 10 nm Ag film, the average diameter was increased to 248.4 nm with a correlation distance of 188.7 nm and an area fraction of 33% due to the insufficient thermal energy. At 800 °C, on the other hand, the agglomeration was excessively enhanced and thus the average diameter of Ag nanoparticles was decreased to 81.4 nm with a correlation distance of 354.7 nm and an area fraction of 8.1%. At a high RTA temperature of 800 °C, the surface of Ag nanopatterns became rough. For 10 nm Ag film after RTA at 600 °C, the average diameter and correlation distance of Ag nanoparticles were 109.2 and 271.6 nm, respectively, with an area fraction of 29.5%. Under the same dewetting condition, there was no largely distinct difference between Ag and Ag/SiO_2 nanopatterns as shown in the (ii) and (vi) of Fig. 1.

The Ag and Ag/SiO_2 nanopatterns were transferred directly onto the Si substrate by the ICP etching process. Figure 2 shows (a) SEM images and (b) reflectance spectra of the etched Si SWSs using the Ag nanopatterns after RTA at 600 °C for Ag films of (i) 5 nm, (ii) 10 nm, and (iii) 15 nm and after RTA at (iv) 400 °C and (v) 800 °C for Ag films of 10 nm. The SEM image of the etched Si SWS using the Ag/SiO_2 nanopattern after RTA at 600 °C for 10 nm Ag film is also shown in (vi) of Fig. 2a. The insets of Fig. 2a show the cross-sectional SEM images of the etched Si SWSs. The etching was performed with 50 W RF power and 100 W ICP power at 10 mTorr. As shown in Fig. 2a, the average heights of etched Si SWSs were obtained as 227.8, 338.7, and 284.8 nm for Ag nanopatterns of (i), (ii), and (iii) of Fig. 1, respectively. The etch rate of Si SWSs is affected mainly by the geometry of nanomask patterns including the diameter, correlation distance, and height of Ag nanoparticles on the Si and SiO_2/Si substrates. The nanopatterns with a higher density resulted in a lower etch rate. For S2 and S6, the highest etch rate was observed. In the case of S5, the Ag nanomask patterns were eroded and lift-off during the ICP etching,

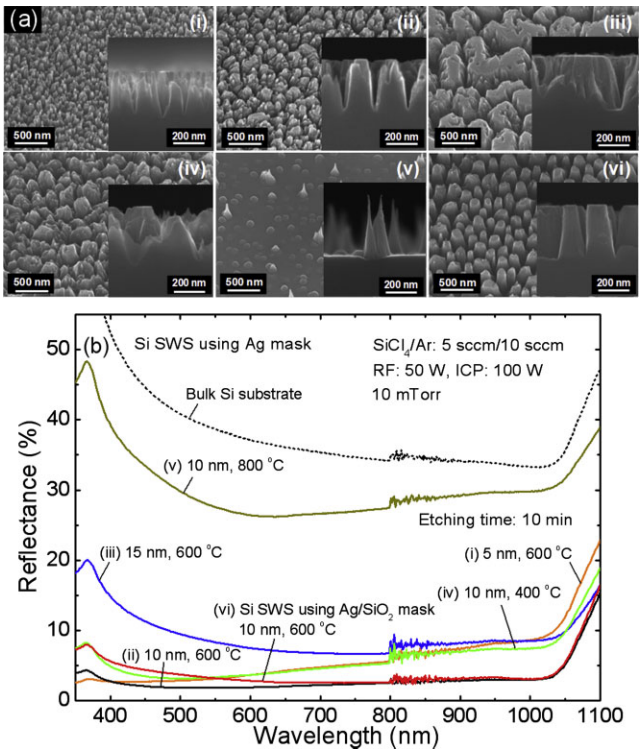

Figure 2 (online color at: www.pss-a.com) (a) SEM images and (b) reflectance spectra of the etched Si SWSs using the Ag nanopatterns after RTA at 600 °C for Ag films of (i) 5 nm, (ii) 10 nm, and (iii) 15 nm and after RTA at (iv) 400 °C and (v) 800 °C for Ag films of 10 nm. The SEM image of the etched Si SWS using the Ag/SiO_2 nanopattern after RTA at 600 °C for 10 nm Ag film is also shown in (vi) of (a). The insets of (a) show the cross-sectional SEM images of the etched Si SWSs.

which sparsely forms several sharp tips. For both Ag and Ag/SiO_2 nanomask patterns, the etch rates were similar. However, more tapered and rough top structures were obtained for Ag nanomask patterns without SiO_2 buffer layer. The reason is that the Ag reacts with etching gas (i.e., $SiCl_4$) [21] and then is partially attacked during the etching. In contrast, for Ag/SiO_2 nanomask patterns, the SiO_2 underlayer still acts as the etch mask despite the attack of Ag nanopatterns.

The total (i.e., specular and diffuse) reflectance was measured by a UV–VIS–NIR spectrophotometer (Carry 5000, Varian) with an integrating sphere for collection of the scattered light at a near normal incidence of $\sim 8^\circ$ using an unpolarized light. The reflectance spectra of the etched Si SWSs are shown in Fig. 2b. For a bulk Si substrate, the reflectance is very high, i.e., $>\sim 30\%$ at wavelengths of 350–1100 nm. The reflectance values of Si SWSs were significantly decreased compared to the bulk Si substrate. For all the samples, the rapid increase in reflectance exists above $\lambda \sim 1030$ nm. This is caused by the backscattering of light by the reflection from the back surface of Si substrates [22]. For S5, the reflectance of the structure was not much reduced, as expected. The S3 etched with large pattern size yielded high

reflectance values of >10% in the short wavelength region. In S2, the use of Ag nanopatterns further lowered the reflectance at wavelengths of 350–700 nm compared to the S6 with Ag/SiO_2 nanopatterns as shown in (ii) and (vi) of Fig. 2b. Clearly, the Si SWSs with a tapered profile exhibit a low reflectance in the short wavelength range [23]. For S1 and S4 with relatively low heights, the reflectance was increased, especially at long wavelengths. Thus, the thermally dewetted Ag nanopatterns after RTA at 600 °C for 10 nm Ag film were optimized as the etch masks for the lowest reflectance of Si SWSs.

Figure 3 shows the reflectance spectra of the etched Si SWSs at different (a) RF powers without ICP power and (b) ICP powers in addition to 50 W RF power at 10 mTorr for the Ag and Ag/SiO_2 nanopatterns after dewetting at 600 °C of 10 nm Ag film. The insets show the SEM images of the etched Si SWSs. The etch rate increased from 2.8 nm/min at 25 W to 21.3 nm/min at 100 W as the RF power increased. The reflectance was gradually decreased with the increase of RF power because the height of the Si SWSs became taller. The Si SWSs etched with Ag nanopatterns exhibited lower reflectance than those with Ag/SiO_2 nanopatterns. As can be seen in the inset of Fig. 3a, the structures show more tapered shapes with rough surfaces for Ag nanopatterns as mentioned above. For S8 and S11 at 50 W RF power, the structures produced effectively the textured profile because of its low etch rate. The texturing was more enhanced in the S8 with Ag nanopatterns, which provides a slightly lower reflectance. Indeed, the tapered structures reduce significantly the reflectance in the short wavelength region. In S9 and S12 at 100 W RF power, the structural collapse occurred and its reflectance was relatively high in the long wavelength region, although it is still lower than the other samples, because the nanopatterns were attacked and lifted off at the high RF power.

The tapered profile as well as the etch rate was further enhanced when the ICP power was applied in addition to the RF power. However, the SWS structures easily collapsed in some regions during the etching with additional ICP power to high RF power. For this reason, a relatively low RF power of 50 W was chosen. The etch rate was increased to 44.9 nm/min at 200 W ICP power and 50 W RF power. It is noted that the etch rate was 12.7 nm/min at only 50 W RF power. For S14, the addition of 200 W ICP power to 50 W RF power also revealed the tapered shapes, as shown in the inset of Fig. 3b, thus leading to the reflectance of <4.1% at 400–1000 nm. By using Ag nanopatterns, the reflectance of S13 was more reduced than that of S4 at wavelengths of <600 nm, indicating a very low reflectance of <~2.4% over a wavelength range of 400–1000 nm. This can explained by the fact that, for the Si SWSs etched using Ag nanopatterns, the effective refractive index profile, based on the volume fraction of the individual constituents [24], is more linearly changed from air to the Si compared to those using Ag/SiO_2 nanopatterns [25, 26].

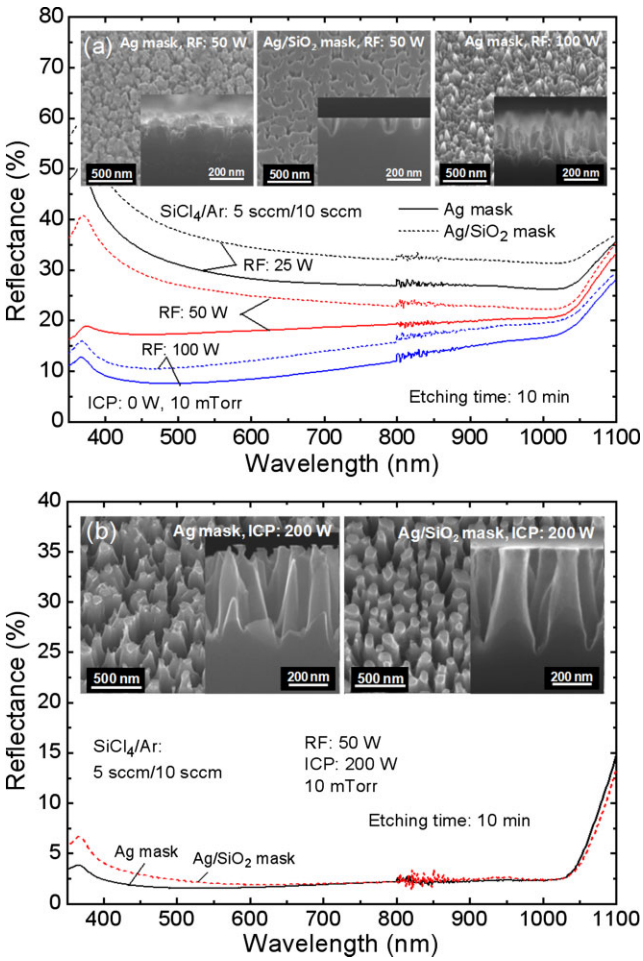

Figure 3 (online color at: www.pss-a.com) Reflectance spectra of the etched Si SWSs at different (a) RF powers without ICP power and (b) ICP powers in addition to 50 W RF power at 10 mTorr for the Ag and Ag/SiO_2 nanopatterns after dewetting at 600 °C of 10 nm Ag film. The insets of (a) and (b) show the SEM images of the etched Si SWSs.

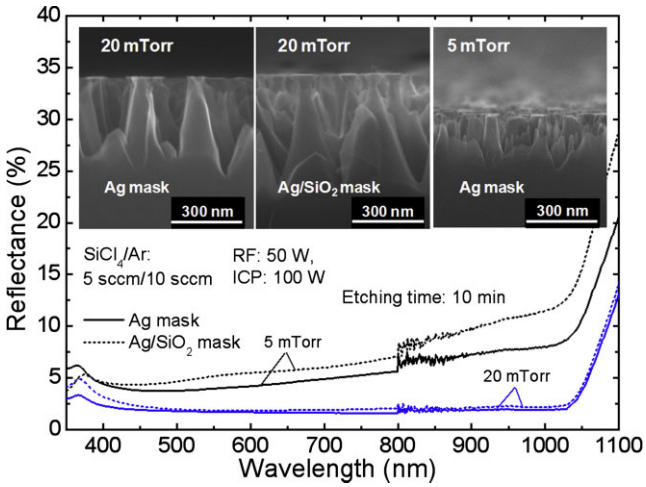

Figure 4 (online color at: www.pss-a.com) Reflectance spectra of the etched Si SWSs with 50 W RF power and 100 W ICP power at process pressures of 5 and 20 mTorr for the Ag and Ag/SiO_2 nanopatterns after dewetting of 600 °C of 10 nm Ag film. The inset shows the SEM images of the etched Si SWSs.

Figure 4 shows the reflectance spectra of the etched Si SWSs at process pressures of 5 and 20 mTorr for the Ag and Ag/SiO_2 nanopatterns after dewetting at 600 °C of 10 nm Ag film. The SEM images of the etched Si SWSs are shown in the insets of Fig. 4. The RF and ICP powers are 50 and 100 W, respectively. The height of SWSs increased as the process pressure increased. When the process pressure was decreased to 5 mTorr (i.e., etch rate of 15.7 nm/min), the reflectance of S15 was increased over a wide wavelength region due to the reduced height of Si SWSs. For S16 and S17 at 20 mTorr, the etch rate was in creased to 42.6 nm/min. For both Ag and Ag/SiO_2 nanopatterns, the etched Si SWSs had tapered profiles due to the enhanced lateral etching, but its top was sharper with a rough surface for S16 with Ag nanopatterns. For S17 with Ag/SiO_2 nanopatterns, the undercut sidewall beneath the etch mask was observed owing to the SiO_2 buffer layer. For S16 with Ag nanopatterns, therefore, the reflectance of the Si SWS was slightly reduced at wavelengths of <500 nm. However, at 20 mTorr, the use of high ICP power, i.e., 200 W, caused a partial collapse of the structure because the erosion of Ag and Ag/SiO_2 nanopatterns during the etching process.

To investigate the angle-dependent antireflection property of the Si SWSs, the unpolarized reflectance was measured using a Cary variable angle specular reflectance accessory in a specular mode. Figure 5 shows the specular reflectance spectra at light incidence angles of $\theta_i = 8$–70° for the Si SWS etched with 50 W RF power and 200 W ICP power at 10 mTorr process pressure. For comparison, the total reflectance spectrum is also shown by the dashed line at a normal incidence of $\theta_i = 8^\circ$. The inset of Fig. 5 shows the photographs of the Si substrate and the corresponding fabricated Si SWSs for Ag and Ag/SiO_2 nanopatterns. As can be seen in the inset of Fig. 5, the surface of the S13 and S14 appeared dark black compared to the Si substrate. This is caused by the reduced surface reflectivity. The S13 was more likely black than that of S14. The specular reflectance was almost the same with the total reflectance at wavelengths of 750–1030 nm though the specular reflectance was slightly lower at wavelengths of <750 nm. At $\lambda > 1030$ nm, there exists the discrepancy caused by the backscattered light as explained in Fig. 2b. The reflectance increased with the increase of incident angle and it was raised rapidly at $\theta_i > 50^\circ$. The reflectance of S13 was maintained at values less than 16% over a wavelength region of 350–1100 nm up to the incident angle of $\theta_i = 50^\circ$, especially <9.9% at $\theta_i = 40^\circ$.

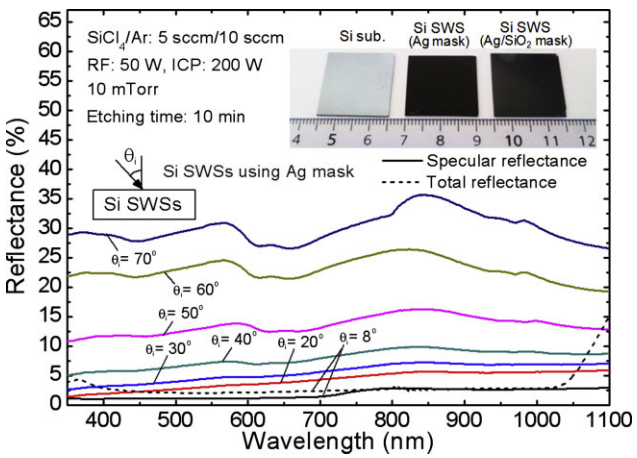

Figure 5 (online color at: www.pss-a.com) Specular reflectance spectra at light incidence angles of $\theta_i = 8$–70° for the Si SWS etched with 50 W RF power and 200 W ICP power at 10 mTorr process pressure. For comparison, the total reflectance spectrum is also shown by the dashed line at a normal incidence of $\theta_i = 8^\circ$. The inset shows the photographs of the Si substrate and the corresponding fabricated Si SWSs for Ag and Ag/SiO_2 nanopatterns.

4 Conclusion We studied the antireflection properties of the disordered Si SWSs on Si substrates via the $SiCl_4/Ar$ ICP etching using thermally dewetted Ag nanopatterns as the etch mask by changing etching process parameters, in comparison with Ag/SiO_2 nanopatterns. With RTA of 10 nm Ag film at 600 °C for 120 s, the geometry of Ag nanopatterns on Si and SiO_2/Si substrates was optimized to obtain the lowest reflectance of Si SWSs. The addition of the ICP power to the RF power reduced significantly the reflectance. At higher process pressure, the reflectance was decreased. The Si SWS etched using Ag nanopatterns at 50 W RF power, 200 W ICP power, and 10 mTorr process pressure exhibited a very low reflectance of $<\sim$2.4% over a wide wavelength range of 400–1000 nm. The Ag nanopatterns, which provide more tapered profiles and rough surfaces of Si SWSs, further improved the antireflection property in the short wavelength region. As a result, the disordered Si SWSs with taller height and tapered profile leads to the relatively low wide-angle reflectance spectra over a broadband wavelength range.

Acknowledgements This research was supported by Basic Science Research Program through the National Research Foundation of Korea (NRF) funded by the Ministry of Education, Science, and Technology (no. 2010-0016930).

References

[1] R. Guntupalli and R. Allen, Proc. SPIE **6294**, 629401 (2006).
[2] C. Lee, S. Y. Bae, S. Mobasser, and H. Manohara, Nano Lett. **5**, 2438 (2005).
[3] J. K. Kim, S. Chhajed, M. F. Schubert, E. F. Schubert, A. J. Fischer, M. H. Crawford, J. Cho, H. Kim, and C. Sone, Adv. Mater. **20**, 801 (2008).
[4] Y. J. Lee, D. S. Ruby, D. W. Peters, B. B. McKenzie, and J. W. P. Hsu, Nano Lett. **8**, 1501 (2008).
[5] P. Lalanne and G. M. Morris, Proc. SPIE **2776**, 300 (1996).
[6] S. Walheim, E. Schaffer, J. Mlynek, and U. Steiner, Science **283**, 520 (1999).
[7] Y. M. Song, S. J. Jang, J. S. Yu, and Y. T. Lee, Small **6**, 984 (2010).
[8] S. L. Diedenhofen, G. Vecchi, R. E. Algra, A. hartsuiker, O. L. Muskens, G. Immink, E. P. A. M. Bakkers, W. L. Vos, and J. G. Rivas, Adv. Mater. **21**, 973 (2009).
[9] J. Zhu, C. M. Hsu, Z. Yu, S. Fan, and Y. Cui, Nano Lett. **10**, 1979 (2010).

[10] Y. M. Song, E. S. Choi, G. C. Park, C. Y. Park, S. J. Jang, and Y. T. Lee, Appl. Phys. Lett. **97**, 093110 (2010).
[11] Y. Kanamori, K. I. Kobayashi, H. Yugami, and K. Hane, Jpn. J. Appl. Phys. **42**, 4020 (2003).
[12] Z. Yu, H. Gao, W. Wu, H. Ge, and S. Y. Chou, J. Vac. Sci. Technol. B **21**, 2874 (2003).
[13] F. Nikolajeff, B. Löfving, M. Johansson, J. Bengtsson, S. Hård, and C. Heine, Appl. Opt. **39**, 4842 (2000).
[14] S. Noach, M. Manevich, N. P. Eisenberg, D. Davidov, M. Klebanov, and V. Lyubin, Opt. Mater. **28**, 1054 (2006).
[15] S. Wang, X. Z. Yu, and H. T. Fan, Appl. Phys. Lett. **91**, 061105 (2007).
[16] K. Nishioka, S. Horitab, K. Ohdaira, and H. Matsumura, Sol. Energy Mater. Sol. Cells **92**, 919 (2008).
[17] J. M. Lee and B. I. Kim, Mater. Sci. Eng. A **449-451**, 769 (2007).
[18] K. C. Sahoo, M. K. Lin, E. Y. Chang, Y. Y. Lu, C. C. Chen, J. H. Huang, and C. W. Chang, Nanoscale Res. Lett. **4**, 680 (2009).
[19] S. K. Lee, G. R. Yi, J. H. Moon, S. M. Yang, and D. J. Pine, Adv. Mater. **18**, 2111 (2006).
[20] D. J. Srolovitz and M. G. Goldiner, J. Miner. Met. Mater. Soc. **47**, 31 (1995).
[21] J. Sun, J. F. Wishart, R. van Eldik, R. D. Shalders, and T. W. Swaddle, J. Am. Chem. Soc. **117**, 2600 (1995).
[22] M. L. Kuo, D. J. Poxson, Y. S. Kim, F. W. Mont, J. K. Kim, E. F. Schubert, and S. Y. Lin, Opt. Lett. **33**, 2527 (2008).
[23] S. A. Boden and D. M. Bagnall, Appl. Phys. Lett. **93**, 133108 (2008).
[24] A. J. Jääskeläinen, K. E. Peiponen, J. Räty, U. Tapper, O. Richard, E. I. Kauppinen, and K. Lumme, Opt. Eng. **39**, 2959 (2000).
[25] Y. Li, J. Zhang, and B. Yang, Nano Today **5**, 117 (2010).
[26] K. C. Sahoo, Y. Li, and E. Y. Chang, IEEE Trans. Electron. Dev. **57**, 2427 (2010).